Fluidization and Flow Regimes of Titaniferous Solids

Adam Luckos* and Paul den Hoed

Mintek, Private Bag X3015, Randburg 2125, South Africa

Physical properties of ilmenite and titania slag particles—properties such as particle density, bulk density, packed-bed voidage and sphericity—have been determined for narrow size fractions ranging from 50 to 850 μm of each material. Particle sphericities measured by image analysis decrease with particle size. A comparison with other techniques shows that image analysis predicts lower values of sphericity. For both materials, the minimum fluidizing velocity, U_{mf}, and transport velocity, U_{tr}, were determined in air at room temperature and atmospheric pressure. The measured minimum fluidizing velocities are higher for ilmenite particles than for slag particles because the density and sphericity of the ilmenite are higher. Separate correlations for U_{mf}, based on a simplified version of the Ergun equation, were fitted for ilmenite and slag particles. Both of these correlations tend to underestimate the minimum fluidizing velocity for small (<50-μm) particles. The experimental values of the transport velocity were fitted to a single equation, which predicts U_{tr} for both materials with a maximum deviation not exceeding 8%. Flow-regime maps for the upward transport of Cl_2−ilmenite and Cl_2−slag systems at 1000 °C and 0.1 MPa were constructed.

Introduction

Titanium dioxide pigments are produced by two different processes, the older sulfate process and the more recent chloride process developed by Du Pont in the 1950s.[1] In the chloride process, which accounts for about 56% of the production capacity of pigments worldwide, titanium-bearing feedstock, typically rutile, titania slag, or a good-quality ilmenite, is reacted with chlorine and coke (hence carbochlorination) in a bubbling fluidized-bed reactor. The carbochlorination is carried out at temperatures of 900−1200 °C and superficial gas velocities ranging from 0.05 to 1.0 m/s. The most significant limitation of this technology is that fines (particles smaller than 100 μm) cannot be used. Furthermore, titaniferous materials containing large amounts of impurities such as CaO, MgO, and MnO tend to sinter because of the accumulation of liquid chlorides in the bed.

Circulating fluidized-bed (CFB) reactors operate at lower solids concentrations (typically 10−200 kg/m^3) and higher superficial velocities (1−10 m/s) than those of bubbling beds. Under these conditions, finer particles (<100 μm) can be treated; the unit is also more tolerant of alkaline-earth-bearing feedstocks. CFB reactors provide an intense environment for gas−solid reactions because mixing is vigorous and heat and mass transfer are high. In theory, the productivity of a CFB chlorinator operating at 1000 °C can be up to 10 times that of bubbling-bed units.

For a given gas−solid system, the onset of fluidization lies at the minimum fluidizing velocity, U_{mf}, and the onset of fast fluidization—the regime in which CFB reactors operate—is marked by the transport velocity, U_{tr}. Both of these velocities are functions of the physical properties of the solid particles and the fluidizing gas.

In this study, an investigation was undertaken to determine the fluidization characteristics of particles of an ilmenite concentrate and a titania slag both produced in South Africa. The ilmenite and slag particles were divided into several narrow size fractions in the range of 50−850 μm. Particle-size distributions (measured by screening), particle and bulk densities, and sphericities (measured by image analysis) were determined for both materials. The minimum fluidizing velocities and transport velocities were measured in air at ambient conditions (86 kPa, 20−26 °C). The correlations derived for U_{mf} and U_{tr} can be used for the modeling and design of fluidized-bed roasters and chlorinators employed in the titanium industry.

The flow-regime maps for the chlorination of ilmenite and slag at 1000 °C and 0.1 MPa in an upward transport reactor are presented. They provide practical information on regime transitions in circulating fluidized beds and transport risers, units that can be used for the production of titanium tetrachloride.

Test Apparatus

Measurements of minimum fluidizing velocities and transport velocities were conducted in a CFB test facility (Figure 1). The facility comprises an 80-mm-i.d., 5-m-tall column (the riser); a solids-return system (a primary cyclone, a recycle hopper, a 50-mm-i.d. standpipe, and an L valve); a secondary cyclone; a plenum chamber; and a distributor plate (a perforated plate with 6% free surface area). The riser, standpipe, and L valve are lengths of transparent PVC tube. The pressure drop across the bed was measured by means of a U-tube water manometer. Rotameters control the flow rate of air entering the riser.

Materials Tested

The present study was conducted with an ilmenite concentrate of beach-sand origin and a titania slag (see Table 1). The action of wind and water in forming the beach-sand deposits produced subrounded particles of ilmenite; crushing, on the other hand, produced angular particles of slag (see Figure 2). The size distribution of

* To whom correspondence should be addressed. Fax: +27-11-793-6241. E-mail: AdamL@mintek.co.za

10.1021/ie030776j CCC: $27.50
Published on Web 06/04/2004

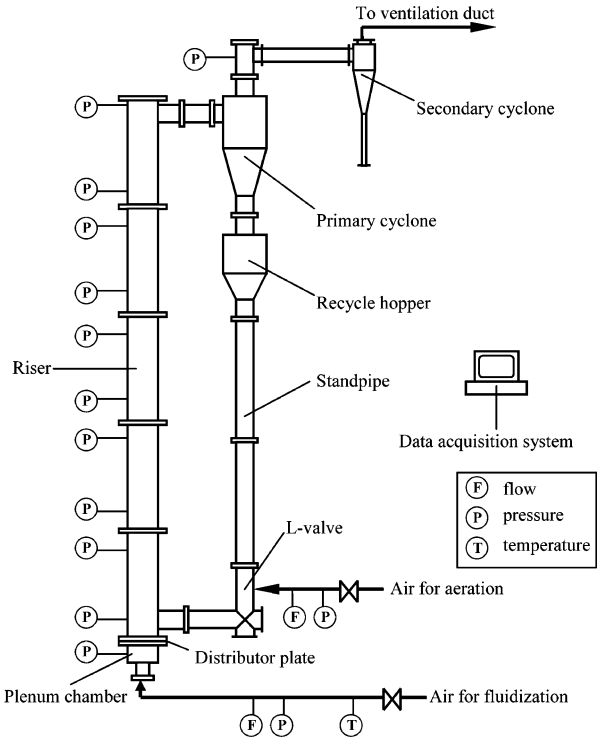

Figure 1. Sketch diagram of the CFB facility.

Table 1. Average Particle Sizes, Particle Densities, and Chemical Compositions of Ilmenite and Titania Slag Samples

	ilmenite	slag
average particle size (μm)	100	205
average particle density (kg/m^3)	4730	4005
chemical composition (mass fraction, %)		
total Ti as TiO_2	47.5	86.0
total Fe as FeO	35.9	9.0
impurities[a]	3.48	7.57

[a] CaO, MgO, MnO, Al_2O_3, Cr_2O_3, SiO_2, V_2O_5 and Nb_2O_5.

each material was measured (Figure 3). Particle sizes of the ilmenite concentrate are more narrowly distributed than those of the slag. Bulk and particle densities were measured; void fractions of the packed beds were calculated from these densities (see Table 2). The samples of material were sieved into five (for ilmenite) and eight (for slag) size fractions. All fractions except the two largest ones of slag belong to group B solids (sand-like particles) according to Geldart's classification.[2] The two largest slag fractions (i.e., 428 and 648 μm) belong to group D.

Test Procedures

Particle Sphericity. Particle sphericity, ϕ_s, is defined as the ratio of the surface area of a sphere to the surface area of a particle having the same volume.[3] Its value falls between 0 and 1—i.e., $0 < \phi_s \leq 1$. In this study, the sphericities of ilmenite and slag particles were determined with the aid of an optical microscope. A Leica Q600 image analyzer measured the projected area (A_i) and projected perimeter (L_i) of particles mounted in polished section, from which the sphericity of particle i was calculated using

$$\phi_{s,i} = \frac{1.064\pi A_i}{L_i^2} \quad (1)$$

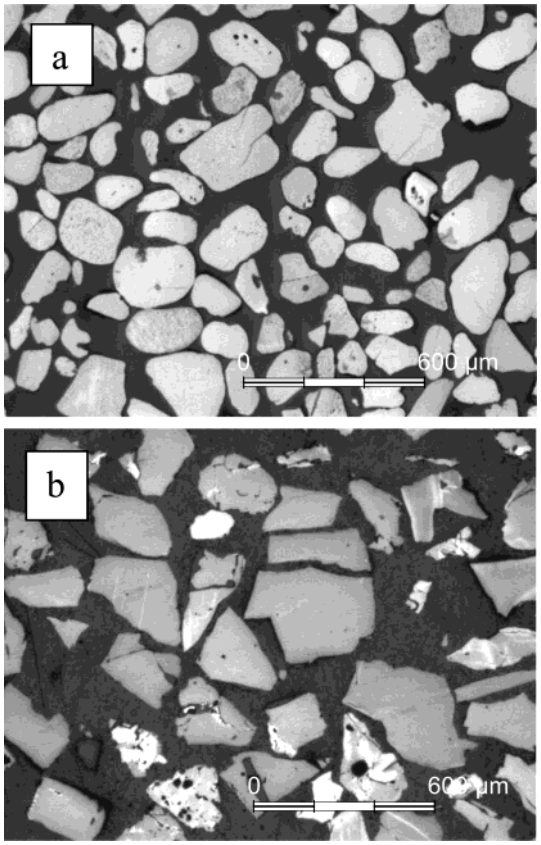

Figure 2. Backscattered-electron images of particles of (a) ilmenite and (b) slag.

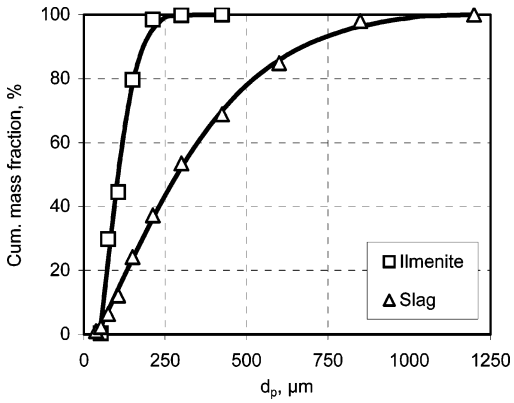

Figure 3. Particle-size distributions for samples of ilmenite and slag.

where 1.064 is a factor compensating for measurements by square pixels. The average sphericity of particles in a size fraction is taken to be the arithmetic mean

$$\phi_s = \frac{1}{N}\sum_i \phi_{s,i} \quad (2)$$

where N is the number of particles counted.

As it stands, the relationship in eq 1 makes an assumption that the measurements over a polished section in two dimensions can be translated to a quantity, ϕ_s, in three dimensions. The validity of this assumption has yet to be demonstrated. We suspect that the technique estimates a value for ϕ_s that is lower than the true value.

Minimum Fluidizing Velocity. The minimum fluidizing velocity, U_{mf}, was determined from measure-

Table 2. Mean Particle Sizes, Particle Densities, Bulk Densities, Packed-Bed Voidages, and Sphericities

size range, $d_{10}-d_{90}$ (μm)	mean particle size, d_p (μm)	particle density,[a] ρ_p (kg/m^3)	bulk density,[b] ρ_b (kg/m^3)	packed-bed voidage,[c] ϵ_o	sphericity, ϕ_s		
					IA	MFV	PD
			Ilmenite				
75−105	89.6	4745	2580	0.456	0.761	0.854	0.851
80−145	107	4745	2612	0.449	0.782	0.854	0.844
85−145	109	4741	2622	0.447	0.793	0.857	0.828
95−195	132	4696	2590	0.448	0.746	0.807	0.762
110−275	174	4674	2608	0.442	0.730	0.784	0.809
			Slag				
55−75	64	4001	1765	0.559	0.656	0.692	0.702
75−105	90.5	3969	1789	0.549	−	0.637	0.565
90−145	113	4006	1844	0.540	0.598	0.621	0.638
120−205	161	4007	1861	0.536	0.533	0.543	0.536
175−290	232	4007	1879	0.531	0.507	0.544	0.509
245−415	331	4011	1914	0.523	0.439	0.555	0.482
325−570	428	4010	1907	0.524	0.456	0.546	0.572
475−845	648	4010	1954	0.513	0.446	0.564	0.489

[a] Measured by helium pycnometer (Micromeritics AccuPyc 1330). [b] Measured by pouring samples into a measuring cylinder and, without compacting, recording the mass of 500 mL. [c] Calculated from particle density and bulk density.

ments of the pressure drop across the bed as a function of the superficial gas velocity. A known mass of sample was charged into the column to a height of approximately 80 mm, which corresponds to a bed aspect ratio (height-to-diameter ratio) of 1. The pressure drop across the bed and distributor plate was measured with a manometer connected to two pressure taps, one located just below the distributor plate and the other above the dense bed. For each sample tested, the gas flow rate was increased from zero until the bed was completely fluidized. The value of U_{mf} coincides with the elbow in the plot of the pressure drop across the bed versus the gas superficial velocity, a change in gradient marked by moving from a packed bed to a fully fluidized one.

Transport Velocity. There is more than one technique for measuring the transport velocities of particles. Those recorded in the literature include determination of the flooding point,[4] determination of the pressure drop at the bottom of the column as a function of the solids circulation flux at different gas velocities,[4] determination of the maximum solids circulation flux at different velocities,[5] and determination of the emptying times of a fast-fluidization column.[6] For Adánez et al.,[7] the last technique is the most attractive because the measurement is simple and quick to conduct. This is the technique we used to measure transport velocities.

The emptying-time technique is based on measurements of the time required for all solids to leave the bed at different settings of the superficial gas velocity. No fresh solids are fed to the column and the L valve is closed. As the gas velocity is increased, a point is reached where the acceleration of the solids increases. In the absence of solids recycling, the bed empties in a short time. The transport velocity, U_{tr}, is taken to be the intersection of the lines of low and high accelerations (see Figure 4). Measurements are not sensitive to the initial mass of solids in the column;[7] all experiments were conducted with samples of 3 kg.

Results and Discussion

Particle Sphericity. As expected, the sphericities of the particles in the ilmenite concentrate, ranging from 0.73 to 0.79, are fairly high (see IA in Table 2). The sphericities of the slag particles are lower and are a function of particle size: they decrease with increasing particle size from 0.66 for 64-μm particles to 0.44 for

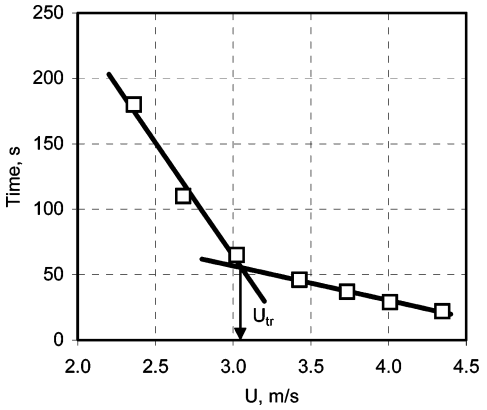

Figure 4. Emptying time as a function of gas velocity for ilmenite with $d_p = 109$ μm.

331-μm particles. The sphericities of the slag particles appear to remain uniform for coarser particles (>300 μm).

To verify measurements obtained optically (IA), we determined sphericity in two other ways. By assuming that $\epsilon_{mf} \approx \epsilon_o$ at minimum fluidization, one can calculate sphericity from a relationship for the minimum fluidizing velocity, U_{mf} (MFV), that is obtained empirically. The relationship is the Ergun equation (see next section), simplified because, for both materials, $Re_{mf} < 20$

$$\phi_s = \sqrt{\frac{150(1-\epsilon_o)}{\epsilon_o^3}\frac{Re_{mf}}{Ar}} \tag{3}$$

A third determination of sphericity derives from measurements of the pressure drop (PD) across a packed bed. By this technique, particle sphericity is calculated from the relationship

$$\phi_s = \sqrt{\frac{150(1-\epsilon_o)^2}{\epsilon_o^3}\frac{\mu U}{d_p^2}\frac{L}{\Delta P}} \tag{4}$$

Sphericities for ilmenite and slag particles as determined by all three techniques are listed in Table 2.

Although the results obtained by these three techniques are scattered, two trends are clearly visible. First, for both materials, IA measurements give the lowest values of ϕ_s for all size fractions. This observation could confirm our suspicion that the IA technique tends

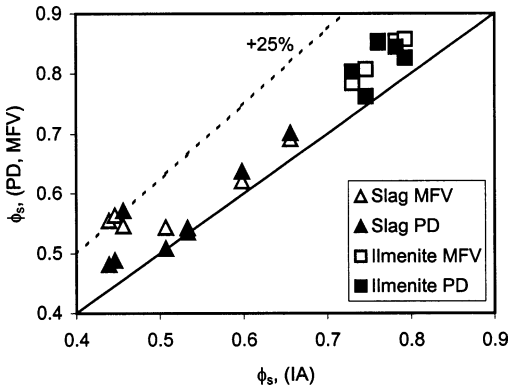

Figure 5. Comparison of measurements by PD and MFV with those by IA.

Table 3. Minimum Fluidizing Velocities and Transport Velocities for Beds of Ilmenite and Slag Particles

	at minimum fluidization			at the transport velocity		
d_p (μm)	U_{mf} (m/s)	Re_{mf}	Ar	U_{tr} (m/s)	Re_{tr}	Ar
			Ilmenite			
89.6	0.017	0.0858	101.3	2.766	14.63	106.3
107	0.023	0.1371	171.8	2.950	18.98	185.9
109	0.024	0.1436	181.4	3.068	19.91	194.8
132	0.031	0.2258	319.2	3.532	27.62	341.6
174	0.048	0.4601	724.6	4.186	46.25	786.6
			Slag			
64	0.011	0.0387	30.57	1.979	7.521	33.23
90.5	0.017	0.0888	89.54	–	–	–
113	0.024	0.1520	172.5	3.236	22.23	191.7
161	0.036	0.3260	499.0	3.912	38.65	561.9
232	0.073	0.9366	1489	5.083	72.11	1672
331	0.145	2.6763	4353	6.251	127.4	4907
428	0.238	5.7472	9582	7.755	200.7	10350
648	0.535	19.461	33125	–	–	–

to underestimate particle sphericity. Determinations of ϕ_s by the PD technique are the most consistent, with the maximum deviation from IA values not exceeding 12% in the case of ilmenite particles and 26% in the case of slag particles (Figure 5). For both materials, the relative deviation increases with particle size.

Second, for both materials, ϕ_s decreases with increasing particle size between 50 and 350 μm. This trend is much more pronounced for slag particles, where ϕ_s drops by 25% from an initial value of 0.68 for 64-μm particles to 0.51 for particles larger than 200 μm. The dependence of sphericity on particle diameter presented in this study runs counter to a trend for lime and limestone particles reported by Pata and Hartman.[8] In their work, however, particle sphericity was determined by a technique proposed by Brown et al.[9] in which measurements were made with beds of monosized particles. In the samples of ilmenite and slag studied here, there is a range of particle sizes within each narrow size fraction tested. The coexistence of fine and coarse particles in the bed results in a bed of lower voidage than that for monosized particles. This explains the observation that beds of large slag particles with low sphericity have lower packed-bed voidages than beds of more rounded small particles (see Table 2).

Minimum Fluidizing Velocity. The minimum fluidizing velocity, U_{mf}, was determined for each size fraction of ilmenite and titania slag (Table 3). The particle Reynolds number at minimum fluidization, Re_{mf}, and the Archimedes number, Ar, were calculated from the physical properties of the system. Figure 6 shows U_{mf} as a function of mean particle diameter.

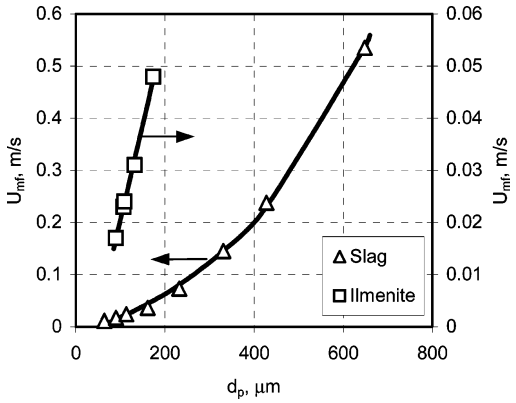

Figure 6. U_{mf} for beds of ilmenite and slag particles.

The Ergun capillary flow model for packed beds[10] is posited on there being two sources of resistance to flow, a viscous resistance denoted by a linear term and an inertial resistance denoted by a quadratic term, with each term expressed with respect to the superficial gas velocity. Applied at the point of minimum fluidization, this semiempirical model[3] finds expression in

$$K_1 Re_{mf}^2 + K_2 Re_{mf} = Ar \tag{5}$$

where

$$K_1 = \frac{1.75}{\epsilon_{mf}^3 \phi_s} \tag{6}$$

and

$$K_2 = \frac{150(1 - \epsilon_{mf})}{\epsilon_{mf}^3 \phi_s^2} \tag{7}$$

In the case of small particles, for which $Re_{mf} < 20$, Kunii and Levenspiel[3] suggest using a simplified form of eq 5, specifically, one that considers only viscous forces

$$Re_{mf} = \frac{1}{K_2} Ar \tag{8}$$

Wen and Yu[11] found that the values of the sphericity-voidage functions K_1 and K_2 are nearly constant for different kinds of particles over a wide range of conditions ($0.001 \le Re_{mf} \le 4000$). An assumption that K_1 and K_2 are constant implies that ϵ_{mf} does not depend on Re_{mf}—a relationship that has not been confirmed empirically. The assumption also implies the existence of "average" values of ϕ_s and ϵ_{mf} that can be used to characterize a bed of nonuniformly sized, irregular particles.

Because U_{mf} is a fundamental variable in the design of fluidized beds, it has been the subject of many empirical studies, usually restricted to specific systems under specific operating conditions. Solving eq 5 for Re_{mf} gives

$$Re_{mf} = \sqrt{C_1^2 + C_2 Ar} - C_1 \tag{9}$$

where

$$C_1 = \frac{K_2}{2K_1} \quad \text{and} \quad C_2 = \frac{1}{K_1} \tag{10}$$

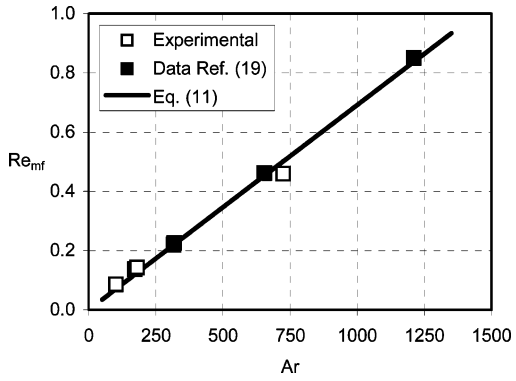

Figure 7. Re_{mf} versus Ar for ilmenite.

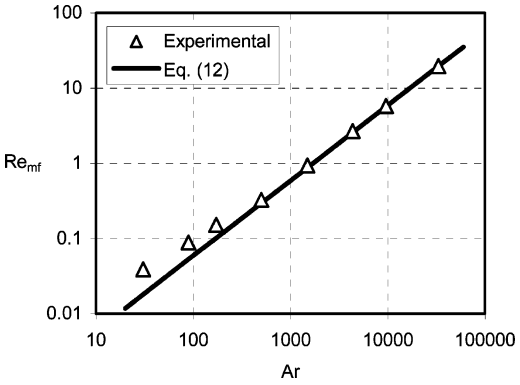

Figure 8. Re_{mf} versus Ar for slag.

Table 4. Coefficients C_1 and C_2 and Derived Average Values of ϵ_{mf} and ϕ_s

study	C_1	C_2	ϵ_{mf}	ϕ_s
Wen and Yu[11]	33.7	0.0408	0.47	0.67
Saxena and Vogel[12]	25.28	0.0571	0.49	0.87
Babu et al.[13]	25.25	0.0651	0.52	0.82
Thonglimp et al.[14]	31.6	0.0425	0.47	0.72
Grace[15]	27.2	0.0408	0.43	0.90
Nakamura et al.[16]	33.95	0.0465	0.51	0.62
Lucas et al.[17]				
$0.8 \le \phi_s \le 1.0$	29.5	0.0357	0.42	0.84
$0.5 \le \phi_s \le 0.8$	32.1	0.0571	0.55	0.60
Wu and Baeyens[18]	30.85	0.0379	0.44	0.78
Sangeetha et al.[19]	15.898	0.0201	0.26	2.00

In the absence of direct measurements of ϕ_s and ϵ_{mf}, most investigators have determined the coefficients C_1 and C_2 by fitting the model (eq 9) to experimental data. The values of these coefficients can be significantly different for different sets of data used for fitting. Table 4 lists the different values of C_1 and C_2 and the corresponding values of average ϕ_s and ϵ_{mf}.

The correlation derived by Sangeetha et al.[19] is incorrect because $\phi_s > 1$. The same can be said of the correlations proposed by Adánez and Abanades[20] and Hartman et al.[21]

The average values of ϕ_s in Table 4 are in the range of 0.60−0.90, which covers those measured by IA for ilmenite particles (0.73−0.793). However, except for $d_p < 113\ \mu$m, the measured values of ϕ_s for slag particles are smaller than the range of values in Table 4.

For beds of slag and ilmenite particles, the relationship between Ar and Re_{mf} is linear (see Figures 7 and 8). Data on U_{mf} reported by Sangeetha et al.[19] for 128-, 163-, and 200-μm ilmenite particles at ambient conditions are also included (Figure 7). Because Re_{mf} is less than 20 for both materials, the experimental results have been modeled using eq 8. The numerical values of constant K_2, the sphericity-voidage function, were determined for both materials by a least-squares regression, giving

$$Re_{mf} = 6.92 \times 10^{-4} Ar \tag{11}$$

for a bed of ilmenite particles and

$$Re_{mf} = 5.89 \times 10^{-4} Ar \tag{12}$$

for a bed of titania slag particles.

Equation 11 predicts higher values of U_{mf} for ilmenite particles because the particle density and sphericity are higher than those of slag particles. For both materials, eqs 11 and 12 underestimate U_{mf} for small particles ($Ar < 200$). The maximum deviation from experimental values is 18.3% for ilmenite and 53.5% for slag. Mean deviations for all measured size fractions are 7.4% for ilmenite and 18.3% for slag particles.

Assuming average sphericities for ilmenite and slag particles of 0.804 and 0.556, respectively—calculated from the data in Table 2—we calculated values of the average voidage at incipient fluidization, ϵ_{mf}, of 0.447 for beds of ilmenite and 0.517 for beds of titania slag. For ilmenite, the calculated average ϵ_{mf} and the average voidage of a packed bed, ϵ_o, are almost identical (see Table 2). This similarity, supported by visual observations, indicates that the bed does not expand (or barely expands) during the transition from a packed state to one that is incipiently fluidized.

For slag, the average ϵ_{mf} approximates ϵ_o for beds of large particles. For beds of fine particles, however, the average ϵ_{mf} is significantly lower than ϵ_o, a discrepancy we attribute to greater uncertainties in our determination of U_{mf}.

Minimum fluidizing velocities calculated from eqs 11 and 12 are higher than those predicted by the correlation proposed by Wen and Yu[11] and lower than those obtained by applying the equation of Lucas et al.[17] for $0.5 \le \phi_s \le 0.8$.

Transport Velocity. Circulating fluidized-bed reactors are operated in a regime identified as fast fluidization; it is a regime of gas−solid fluidization covering a range of velocities above the transport velocity. The transport velocity, U_{tr}, is an important design parameter because it marks the minimum gas velocity required for a CFB reactor to run in a stable manner. Transport velocities determined empirically for size fractions of ilmenite and titania slag particles are listed in Table 3 together with corresponding values of Ar and Re_{tr}. U_{tr} increases almost linearly with mean particle diameter (Figure 9).

Transport velocity has been the subject of a number of empirical studies conducted with group A and group B materials at ambient conditions. Smolders and Baeyens[22] recently reviewed the techniques used, the relevant solids properties, the results of measurements, and the available correlations. Perales et al.[23] demonstrated that variations in transport velocity conform to the following empirical relationship

$$Re_{tr} = aAr^b \tag{13}$$

where a and b are constant. Several studies have determined values for a and b (see Table 5). Bi et al.[27] point out that it is difficult to judge which correlation best predicts U_{tr} because the experimental data are too

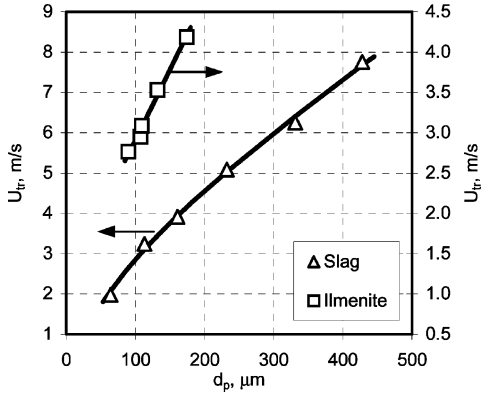

Figure 9. Transport velocities for ilmenite and slag particles.

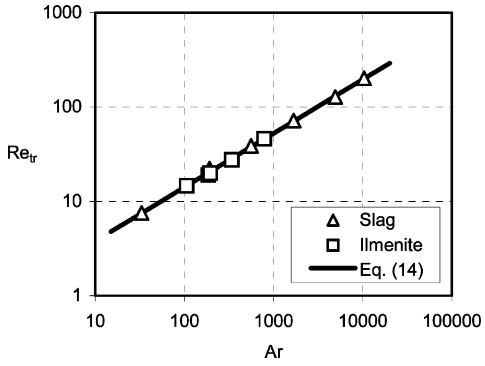

Figure 10. Relationship between Re_{tr} and Ar for ilmenite and slag particles.

Table 5. Correlations for U_{tr}

authors	*a*	*b*
Adanez et al.[7]	2.078	0.463
Smolders and Baeyens[22]	1.75	0.468
Perales et al.[23]	1.45	0.484
Mori et al.[24]	1.41	0.56
Bi and Fan[25]	2.28	0.419
Lee and Kim[26]	2.916	0.345

widely scattered and the uncertainty, consequently, too great. This scatter can be attributed to several factors, including experimental technique, differences in the locations of measurement points, and equipment size.

In this study, eq 13 has been used to correlate experimental data obtained for ilmenite and slag particles (Figure 10). The values of constants *a* and *b* were found by a least-squares regression of the data for both materials

$$Re_{tr} = 1.013Ar^{0.572} \tag{14}$$

Re_{tr} calculated in eq 14 deviates from experimental values with a mean of 2.6% and maximum of less than 8%.

Among the correlations listed in Table 5, the equation proposed by Mori et al.[24] predicts the highest values of U_{tr}, and that proposed by Lee and Kim[26] predicts the lowest ones. Transport velocities calculated from eq 14 lie between these two extremes.

Flow-Regime Diagrams

Flow-regime maps provide information about the nature of gas−solid flow for a given gas−solid system in a vertical tube in which gas flows from bottom to top. They identify three regimes for the operation of CFBs,

Table 6. Correlations Relating to the Flow-Regime Maps

ref	equation	eq no.
28	$V_{mf} = U_{mf} + \frac{G_s\epsilon_{mf}}{\rho_p(1-\epsilon_{mf})}$	15
28	$V_C = U_C + \frac{G_s\epsilon_C}{\rho_p(1-\epsilon_C)}$	16
29	$\epsilon_C = \epsilon_{BC} + (1-\epsilon_{BC})\epsilon_{mf}$	17
29	$\epsilon_{BC} = 0.30Ar^{0.04} \qquad 2 < Ar < 2\times10^6$	18
30	$\frac{V_{CC}}{\sqrt{gd_p}} = \frac{32}{Re_t^{0.06}}\left(\frac{G_s}{\rho V_{CC}}\right)^{0.28}$	19
31	$Re_t = U_t^* Ar^{1/3}$	20
31	$U_t^* = \left[\frac{18}{(d_p^*)^2} + \frac{2.335 - 1.744\phi_s}{\sqrt{d_p^*}}\right]^{-1} \qquad 0.5 \le \phi_s \le 1$	21
31	$d_p^* = Ar^{1/3}$	22
28	$V_{CA} = U_{se} + \frac{G_s\epsilon_{CA}}{\rho_p(1-\epsilon_{CA})}$	23
32	$Re_{se} = 1.53Ar^{0.5} \qquad 2 < Ar < 4\times10^6$	24
33	$V_{mp} = 10.1\frac{(gd_p)^{0.347}}{Ar^{0.021}}\left(\frac{G_s}{\rho}\right)^{0.31}\left(\frac{d_p}{D}\right)^{-0.139}$	25

namely, (1) one in which gas and solids move cocurrently in the upward direction (homogeneous dilute-phase flow), (2) one in which the upward flow of gas and solids is accompanied by significant downward flow of solids at the wall (core−annular dilute-phase flow), and (3) one in which the axially uniform suspension of core−annular flow has collapsed so that a collapsed dense phase forms at the bottom of the column and core−annular flow persists in the upper section (fast fluidization). Bi and Grace[28] constructed the boundaries between these regimes using correlations listed in Table 6. The important ones for our purposes are eqs 25, 23, and 19, which give V_{mp}, V_{CA}, and V_{CC}, respectively. Circulating fluidized beds are operated at gas velocities between the velocity at minimum pressure gradient (V_{mp}) and the type-C choking velocity (V_{CC}).

Using the correlations recommended by Bi and Grace,[28] we have constructed flow-regime maps for particles of ilmenite and titania slag undergoing chlorination in a CFB at 1000 °C and 100 kPa. In using the correlations listed in Table 6, we have substituted in the parameters of these correlations values for the properties of ilmenite, slag and chlorine and for the riser diameter.

The maps appear in Figure 11. They provide practical information on flow regimes in the CFB chlorinator constructed at Mintek (see Luckos and Mitchell[34]). Note that, for dilute-phase flow, the boundary between core−annular flow and homogeneous flow depends on the diameter of the column. The other boundaries do not have this dependence.

In comparing graphs a and b of Figure 11, one can see that the range of operating velocities for core−annular dilute-phase flow is narrower for coarser particles; the range of operating velocities for fast fluidization becomes correspondingly wider. The hatched areas indicate regimes where the solids circulation flux, G_s, can no longer be sustained. The circulation of solids

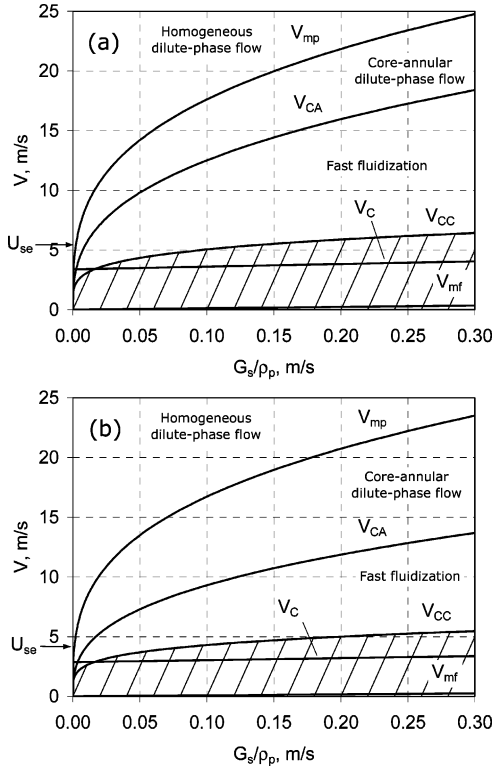

Figure 11. Flow-regime maps for gas−solid upward transport: (a) ilmenite, $d_p = 100\ \mu$m, $\rho_p = 4730$ kg/m^3; (b) slag, $d_p = 200\ \mu$m, $\rho_p = 4005$ kg/m^3.

consequently drops to a value corresponding to the saturated carrying capacity. Finally, as U_{se} intersects the regime for fast fluidization, it is possible to operate the CFB at Mintek in the fast-fluidization regime at velocities less than U_{se}.

Conclusions

This paper reports on the physical properties and fluidization characteristics of two feedstocks, namely, ilmenite and titania slag, that are used in the production of titania pigments by the chloride process. It was found that, for both materials, sphericity decreases with increasing particle size. This observation contradicts some published results based on the sphericity-voidage diagram developed for uniformly sized particles. It appears that the image-analysis technique produces values of sphericity that are lower than those obtained by pressure-drop and minimum-fluidizing-velocity measurements.

Minimum fluidizing velocities and transport velocities were determined for narrow size fractions of each material. Because $Re_{mf} < 20$ for both materials, a simplified version of the Ergun equation that takes into account only viscous forces (eq 8) was used to correlate experimental results. For particles of similar size, those of ilmenite have higher U_{mf} values than those of slag because they are denser and more spherical.

Transport velocities were determined by the emptying-time technique. Correlation eq 14 predicts U_{tr} for both materials with a maximum relative deviation from experimental results not exceeding 8%.

The flow-regime maps, which provide practical information on the flow of ilmenite and slag particles in a CFB chlorinator, show that fast fluidization does exist for superficial gas velocities less than U_{se} and that the annular flow regime becomes narrower for larger particles.

Acknowledgment

We are grateful to the South African National Research Foundation for financial support through its Innovation Fund.

Nomenclature

Ar = Archimedes number, $Ar = d_p^3(\rho_p - \rho)\rho g/\mu^2$
a = constant in eq 13
b = constant in eq 13
d_p = mean particle diameter, m
d_p^* = dimensionless particle diameter eq 22
D = diameter of riser, m
G_s = solids circulation flux, kg/m^2·s
g = acceleration due to gravity, m/s^2
K_1, K_2 = sphericity-voidage functions in eq 5
L = height of the packed bed, m
Re_{mf} = Reynolds number at minimum fluidization, $Re_{mf} = U_{mf}d_p\rho/\mu$
Re_{se} = Reynolds number at U_{se}, $Re_{se} = U_{se}d_p\rho/\mu$
Re_t = Reynolds number at terminal velocity, $Re_t = U_t d_p\rho/\mu$
Re_{tr} = Reynolds number at transport velocity, $Re_{tr} = U_{tr}d_p\rho/\mu$
U = superficial gas velocity, m/s
U_C = transition velocity, m/s
U_{mf} = minimum fluidizing velocity, m/s
U_{se} = velocity at the onset of significant solids entrainment, m/s
U_t = terminal velocity, m/s
U_t^* = dimensionless terminal velocity eq 21
U_{tr} = transport velocity, m/s
V_C = transition velocity in solids transport systems, m/s
V_{CA} = type-A choking velocity, m/s
V_{CC} = type-C choking velocity, m/s
V_{mf} = the minimum fluidizing velocity in solids transport systems, m/s
V_{mp} = minimum pressure gradient velocity, m/s

Greek Letters

ΔP = pressure drop across the bed, Pa
ϵ_o = packed-bed voidage
ϵ_{BC} = bubble-phase volume fraction at the transition point
ϵ_C = voidage at the transition point
ϵ_{mf} = voidage at minimum fluidization
ϕ_s = sphericity
ρ = gas density, kg/m^3
ρ_b = bulk density, kg/m^3
ρ_p = solids density, kg/m^3
μ = gas viscosity, kg/m·s

Literature Cited

(1) Woditsch, P.; Westerhaus, A. Pigments, Inorganic: Titanium Dioxide. In *Ullmann's Encyclopedia of Industral Chemistry*; Gerhartz, W., Yamamoto, Y. S., Campbell, F. T., Pfefferkorn, R., Rounsaville, J. F., Eds.; VCH Verlagsgesselschaft: Weinheim, Germany, 1985; Vol. A20.

(2) Geldart, D.; Abrahamsen, A. R. Homogeneous Fluidization of Fine Powders Using Various Gases and Pressures. *Powder Technol.* **1978**, *19*, 133.

(3) Kunii, D.; Levenspiel, O. *Fluidization Engineering*, 2nd ed.; Butterworth-Heinemann: Boston, 1991.

(4) Yerushalmi, J.; Cankurt, N. T. Further Studies of the Regimes of Fluidization. *Powder Technol.* **1979**, *24*, 187.

(5) Schnitzlein, M. G.; Weinstein, H. Flow Characterization in High-Velocity Fluidized Beds Using Pressure Fluctuations. *Chem. Eng. Sci.* **1988**, *43*, 2605.

(6) Han, G. Y.; Lee, G. S.; Kim, S. D. Hydrodynamics of a Circulating Fluidized Bed. *Korean J. Chem. Eng.* **1985**, *2*, 141.

(7) Adánez, J.; de Diego, L. F.; Gayán, P. Transport Velocities of Coal and Sand Particles. *Powder Technol.* **1993**, *77*, 61.

(8) Pata, J.; Hartman, M. Minimum Fluidization Velocities of Lime and Limestone Particles. *Ind. Eng. Process Des. Dev.* **1978**, *17*, 231.

(9) Brown, G. G.; Foust, A. S.; Brown, G. M.; La Verne Katz, D.; Brownell, L. E.; Schneidewind, R.; Martin, J. J.; White, R. R.; Williams, G. B.; Wood, W. P.; Banchero, J. T.; York, J. L. *Unit Operations*; John Wiley & Sons: New York, 1950.

(10) Ergun, S. Fluid Flow Through Packed Columns. *Chem. Eng. Prog.* **1952**, *48*, 89.

(11) Wen, C. Y.; Yu, Y. H. A Generalized Method for Predicting the Minimum Fluidization Velocity. *AIChE J.* **1966**, *12*, 610.

(12) Saxena, S. C.; Vogel, G. J. The Measurement of Incipient Fluidisation Velocities in a Bed of Coarse Dolomite at Temperature and Pressure. *Trans. Inst. Chem. Eng.* **1977**, *55*, 184.

(13) Babu, S. P.; Shah, B.; Talwalkar, A. Fluidization Correlations for Coal Gasification Materials—Minimum Fluidization Velocity and Fluidized Bed Expansion Ratio. *AIChE Symp. Ser.* **1978**, *74*, 176.

(14) Thonglimp, V.; Hiquily, N.; Laguerie, C. Vitesse minimale de fluidisation et expansion des couches fluidisées par un gaz. *Powder Technol.* **1984**, *38*, 233.

(15) Grace, J. R. Fluidized Bed Hydrodynamics. In *Handbook of Multiphase Systems*; Hetsroni, G., Ed.; Hemisphere: Washington, DC, 1982.

(16) Nakamura, M.; Hamada, Y.; Toyama, S.; Fouda, A. E.; Capes, C. E. An Experimental Investigation of Minimum Fluidization Velocity at Elevated Temperatures and Pressures. *Can. J. Chem. Eng.* **1985**, *63*, 8.

(17) Lucas, A.; Arnaldos, J.; Casal, J.; Puigjaner, L. Improved Equation for the Calculation of Minimum Fluidization Velocity. *Ind. Eng. Chem. Process Des. Dev.* **1986**, *25*, 426.

(18) Wu, S. Y.; Baeyens, J. Effect of Operating Temperature on Minimum Fluidization Velocity. *Powder Technol.* **1991**, *67*, 217.

(19) Sangeetha, V.; Swathy, R.; Narayanamurthy, N.; Lakshmanan, C. M.; Miranda, L. R. Minimum Fluidization Velocity at High Temperatures Based on Geldart Powder Classification. *Chem. Eng. Technol.* **2000**, *23*, 713.

(20) Adánez, J.; Abanades, J. C. Minimum Fluidization Velocities of Fluidized-Bed Coal-Combustion Solids. *Powder Technol.* **1991**, *67*, 113.

(21) Hartman, M.; Trnka, O.; Svoboda, K. Fluidization Characteristics of Dolomite and Calcined Dolomite Particles. *Chem. Eng. Sci.* **2000**, *55*, 6269.

(22) Smolders, K.; Baeyens, J. Gas Fluidized Beds Operating at High Velocities: A Critical Review of Occurring Regimes. *Powder Technol.* **2001**, *119*, 269.

(23) Perales, J. F.; Coll, T.; Llop, M. F.; Puigjaner, L.; Arnaldos, J.; Casal, J. On the Transition from Bubbling to Fast-Fluidization Regimes. In *Circulating Fluidized Bed Technology III*; Basu, P., Horio, M., Hasatani, M., Eds.; Pergamon Press: Oxford, U.K., 1991; p 73.

(24) Mori, S.; Hashimoto, O.; Haruta, T.; Mochizuki, K.; Matsutani, W.; Hiraoka, S.; Yamada, I.; Kojima, T.; Tuji, K. Turbulent Fluidization Phenomena. In *Circulating Fluidized Bed Technology II*; Basu, P., Large, J. F., Eds.; Pergamon Press: Oxford, U.K., 1988; p 105.

(25) Bi, H.; Fan, L. S. Existence of Turbulent Regime in Gas−Solid Fluidization. *AIChE J.* **1992**, *38*, 297.

(26) Lee, G. S.; Kim, S. D. Bed Expansion Characteristics and Transition Velocity in Turbulent Fluidized Beds. *Powder Technol.* **1990**, *62*, 207.

(27) Bi, H. T.; Ellis, N.; Abba, I. A.; Grace, J. R. A State-of-the-Art Review of Gas−Solid Turbulent Fluidization. *Chem. Eng. Sci.* **2000**, *55*, 4789.

(28) Bi, H. T.; Grace, J. R. Flow Regime Diagrams for Gas−Solid Fluidization and Upward Transport. *Int. J. Multiphase Flow* **1995**, *21*, 1229.

(29) Bi, H. T.; Grace, J. R. Transition from Bubbling to Turbulent Fluidization. Presented at the AIChE Annual Meeting, San Francisco, CA, Nov 13−18, 1994.

(30) Yousfi, Y.; Gau, G. Aerodynamique de l'Ecoulement Vertical de Suspensions Concentrees Gaz−Solides—I. Regimes d'Ecoulement et Stabilite Aerodynamique. *Chem. Eng. Sci.* **1974**, *29*, 1939.

(31) Haider, A.; Levenspiel, O. Drag Coefficient and Terminal Velocity of Spherical and Nonspherical Particles. *Powder Technol.* **1989**, *58*, 63.

(32) Bi, H. T.; Grace, J. R. Regime Transitions Affecting Gas−Solids Suspensions and Fluidized Beds. *Trans. Inst. Chem. Eng.* **1995**, *73* (Part A), 154.

(33) Bi, H. T.; Fan, L.-S. Regime Transitions in Gas−Solid Circulating Fluidized Beds. Presented at the AIChE Annual Meeting, Los Angeles, CA, Nov 18−22, 1991.

(34) Luckos, A.; Mitchell, D. The Design of a Circulating Fluidized-bed Chlorinator at Mintek. In *IFSA 2002 Industrial Fluidization South Africa*; Luckos, A., den Hoed, P., Eds.; SAIMM: Johannesburg, South Africa, 2002; p 147.

Received for review October 16, 2003
Revised manuscript received April 26, 2004
Accepted April 27, 2004

IE030776J